Seismic imaging of structural heterogeneity in Earth's mantle: Evidence for large-scale mantle flow

Jeroen Ritsema and Hendrik-Jan van Heijst
Seismological Laboratory, California Institute of Technology, Pasadena, USA[1]

Systematic analyses of earthquake-generated seismic waves have resulted in models of three-dimensional elastic wave speed structure in Earth's mantle. This paper describes the development and the dominant characteristics of one of the most recently developed models. This model is based on seismic wave travel times and wave shapes from over 100,000 ground motion recordings of earthquakes that occurred between 1980 and 1998. It shows signatures of plate tectonic processes, and it demonstrates the presence of large-scale structure throughout the lower 2000 km of the mantle. Seismological analyses make it increasingly more convincing that geologic processes shaping Earth's surface are intimately linked to physical processes in the deep mantle.

[1]To appear in the Fall 2000 issue of *Science Progress*

1 Introduction

The Earth is a dynamically active planet that is constantly reshaped by geologic processes. Mountain building, volcanism, and earthquake faulting are textbook examples of physical processes related to the motions of large lithospheric plates (the outermost 100–200 km of the mantle) over Earth's surface. However, flow in the Earth's mantle is not confined to the outermost 200-300 km. Plate tectonics is just the top boundary manifestation of large-scale circulation throughout the 3000-km thick mantle, driven by the production of heat within the Earth's deep interior that cannot escape by conduction alone. Precisely in what configuration large-scale circulation is taking place, and to what extent geologic processes at the Earth's surface are linked to processes deep in the mantle remain questions that are vigorously researched. Fundamental constraints on mantle convection such as the amount of heat transferred from the outer core (a liquid Fe–Ni alloy) into the solid silicate mantle, the rheological properties (e.g. viscosity) of the mantle, and whether mid-mantle boundaries partition convection into a multiple layered system are uncertain, yet our understanding of mantle convection and our understanding of the Earth's evolution depend critically on them[1].

Our understanding of global geophysical processes has benefited from advances in the study of the Earth's magnetic and gravity field, laboratory experiments on rock minerals at deep mantle conditions, and computer modeling of convection. However, by far the most stringent constraints on the structure and processes in the Earth's deep interior have come from the study of seismic waves that are generated by earthquakes. Elastic wave speed structure constrained by seismological analyses is an excellent indicator of compositional and temperature variations in the mantle and models of the elasticity of the Earth's mantle are frequently used to infer a present-day snapshot of convection in the Earth's mantle[2].

1.1 Radially symmetric Earth models

To first order, seismic wave propagation in the Earth can be explained by models that describe seismic wave speed as a function of depth only. The Preliminary Reference Earth Model (PREM)[3] is a radially

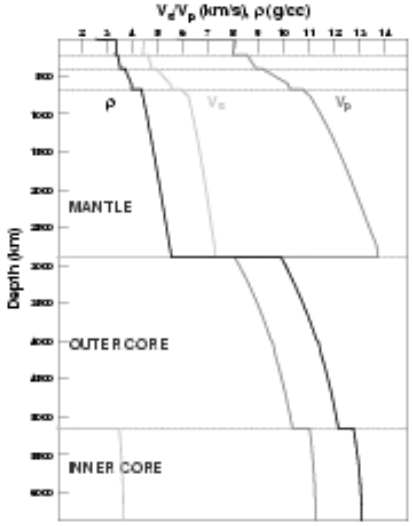

Figure 1: Preliminary Reference Earth Model (PREM) describing density (ρ), shear wave velocity (V_s), and compressional wave velocity (V_p) as a function of depth.

symmetric model of seismic wave speed and density in the Earth that is widely used to study seismic ground motion recordings (Figure 1). At the core-mantle boundary (at a depth of 2890 km), the density

increases discontinuously while P wave velocity decreases discontinuously and the S wave velocity drops to 0. Additional density and wave speed discontinuities in the upper 670 km of the mantle ('upper mantle') reflect the presence of solid-solid phase transitions[4]. Between chemical and phase transitions, the seismic wave speed and density increase smoothly with depth primarily due to adiabatic compression.

The similarity of the ground motion recording of the May 21, 1998 Indonesia earthquake at seismic station TSUM and the synthetic seismogram computed for the PREM model underscores that the main characteristics of seismic waves can be explained by the PREM model (Figure 2). The propagation times of

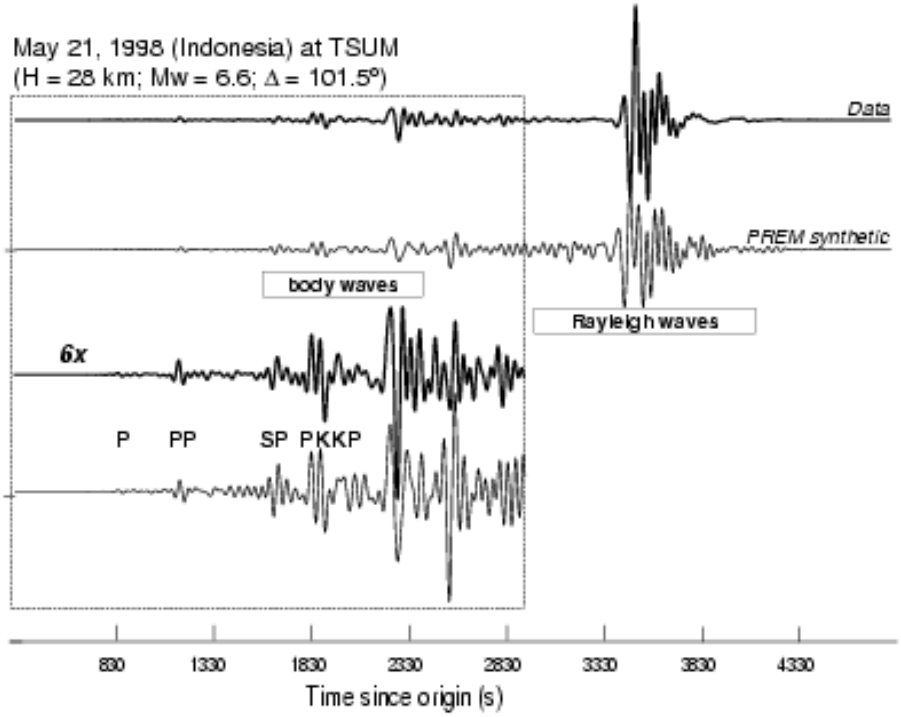

Figure 2: Ground motion recording (thick line) of the May 21, 1998 Indonesia earthquake at station TSUM (Tsumeb, Namibia) and the synthetic seismogram (thin line) computed for the PREM model. The recording shows the oscillatory Rayleigh wave train and relatively 'impulsive' body wave signals which represent wave interactions of 'P' and 'S' waves with Earth's surface and/or the core-mantle boundary. The body wave part of the seismogram is shown at the bottom after it has been amplified by a factor of 6. Various high-amplitude body wave phases are indicated by their phase names.

seismic body waves waves, which propagate through the Earth's deep interior, range from 10 to 30 minutes. These times are predicted by the PREM model to within 10 s. In addition, the dispersion of surface waves, which propagate primarily through the upper mantle, is reproduced accurately by synthetic waveforms computed using the PREM model. This implies that three-dimensional (3-D) variations of seismic wave speed in the mantle and core with respect to the PREM model are small (< 5–10%) and that they affect seismic wave propagation little.

The 3-D variations of seismic wave speed can be regarded as perturbations to a radially symmetric reference model such as PREM and analyzed under the assumption that seismic wave propagation can, to first order, be described using the PREM model. This approximation forms the basis of seismic tomography.

1.2 3-D variations of wave speed in the mantle

Seismic tomography involves the inversion of seismic data for 3-D wave speed variations. In this technique, seismic wave travel times and waveforms are related to the average seismic wave speed along the propagation path. Typically, a large number and diverse types of seismic waves are used. The first tomographic models of the mantle based on seismic waveform data were derived in the early 1980s[5–7], a few years after the deployment of digital seismic instrumentation in worldwide networks began. Even the first tomographic models provided a clear global perspective of seismic heterogeneity in the mantle outlining disparate structures beneath continents and oceans and the predominantly long-wavelength heterogeneity in the deep mantle. As

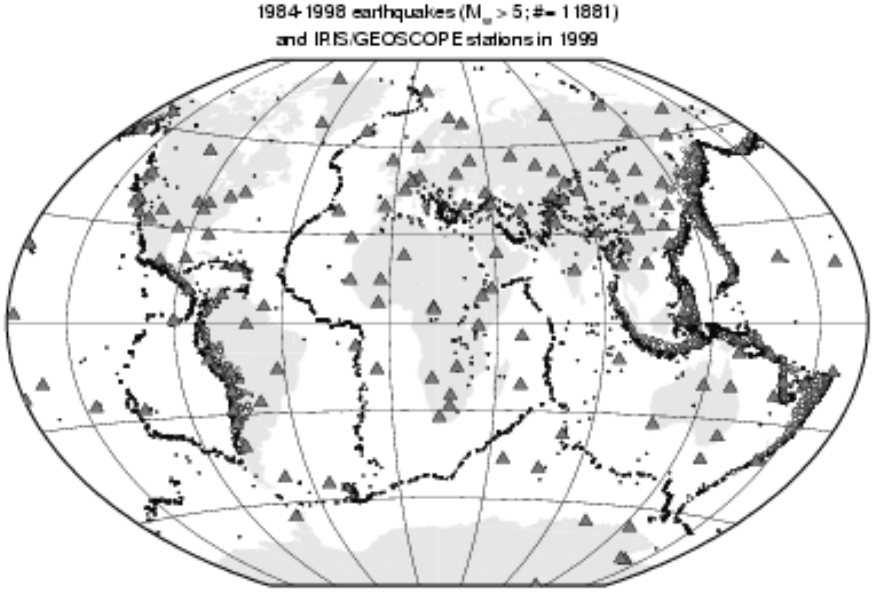

Figure 3: Epicenters of 11191 shallow (0–100 km) earthquakes (small black circles), intermediate-depth (100–300 km) earthquakes (grey circles), and deep (300–700 km) earthquakes (white circles) with magnitudes larger than 5 which occurred between 1984 and 1998. Black triangles indicate the location of digital, global network stations from the IRIS and GEOSCOPE networks presently operating.

networks of seismic stations expanded in the past 20 years (Figure 3) and collections of seismic waveform data grew, the spatial resolution of 3-D whole-mantle models has steadily increased[8–13] and the depth extent of seismic velocity heterogeneity in the upper and lower mantle has been better constrained. At the same time, recent high-resolution models of more localised regions have provided tighter constraints on the thickness of the continental and oceanic lithosphere[14,15] and sharper images of the mantle beneath subduction zone regions[16] and mid-ocean spreading ridges[17].

This paper reviews the construction and characteristics of a new global seismic model, S20RTS[18,19]. The development of this model is based on existing tomographic inversion procedures. However, S20RTS distinguishes itself from previous tomographic experiments by the use of several new seismic wave types, data analysis that incorporates ground motion recordings of earthquakes until 1998, and denser spatial parameterisation.

2 Seismic data

Model S20RTS is a shear velocity model of the mantle based on: (1) Raleigh wave phase velocities, (2) Travel times of shear wave phases, and (3) Splitting parameters of the Earth's free-oscillations.

Figure 4: Ray paths for the phases S, SS, SSS (left), ScS, ScS_2, ScS_3 (middle), SKS, and SKKS (right).

2.1 Shear wave travel times

Shear wave phases are body wave phases that propagate through the mantle with the shear wave speed. We have made travel time measurements of shear wave phases which:

- propagate through the lower mantle (S) or diffract along the core-mantle boundary (S_{diff}),
- reflect once (SS), twice (SSS), or three times (SSSS) off the Earth's surface,
- reflect once (ScS), twice (ScS_2), or three times (ScS_3) off the core-mantle boundary, or
- propagate as compressional waves through the core (SKS and SKKS).

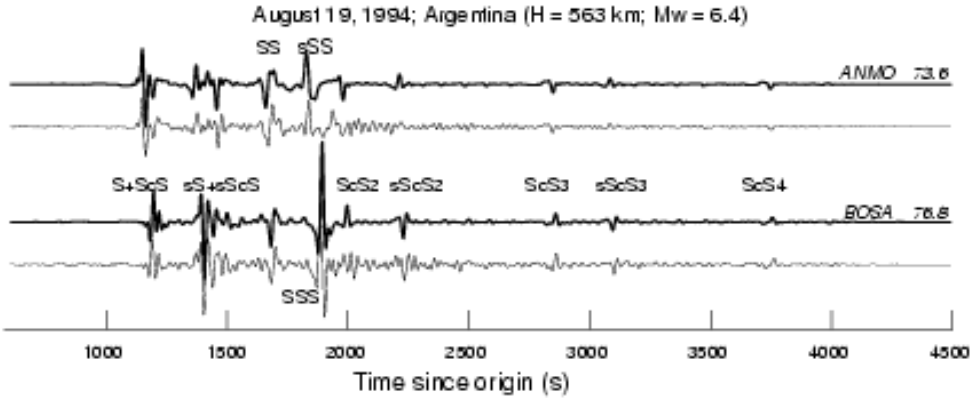

Figure 5: Comparison of transverse component seismograms (thick lines) of the August 19, 1994 Argentina earthquake at stations ANMO (Albuquerque, USA; distance of 73.6°) and BOSA (Boshof, South Africa; distance of 76.8°) with seismograms computed for the PREM model (thin lines). These ground motion recordings show a long sequence of seismic pulses caused by the interaction of S waves with Earth's surface and/or the core-mantle boundary. Phase codes (e.g., S, sSS, ScS3) are plotted at several high-amplitude shear wave phases.

These phases traverse the mantle along very different paths, as is demonstrated by their geometric ray paths shown in Figure 4.

Shear wave travel time anomalies with respect to the PREM model are measured by waveform fitting. In this procedure, we determine the time shift that optimises the match between the waveform of a high amplitude-body wave signal in a ground motion recording and the waveform computed for the PREM model. We apply this technique after the ground motion recordings have been filtered so that only seismic signals with frequencies lower than 0.06 Hz (T > 15 s) are retained. At these relatively low frequencies, the wave shape of recorded and synthesized body waves are similar (Figure 5) because micro-seismic noise is suppressed and shear waves are not complicated by effects of the earthquake rupture process or small-scale (< 100 km) structure.

2.2 Rayleigh wave phase velocity measurements

Rayleigh waves are seismic surface waves that propagate through the upper mantle. Rayleigh waves are sensitive to seismic velocity structure in the upper mantle over a relatively broad depth range (Figure 6). Long-period Rayleigh waves propagate faster than shorter period Rayleigh waves because they are affected by structure at greater depth where wave speeds are higher. Because of the frequency dependence of Rayleigh wave phase velocity, $c(\omega)$, Rayleigh waveforms are strongly dispersed.

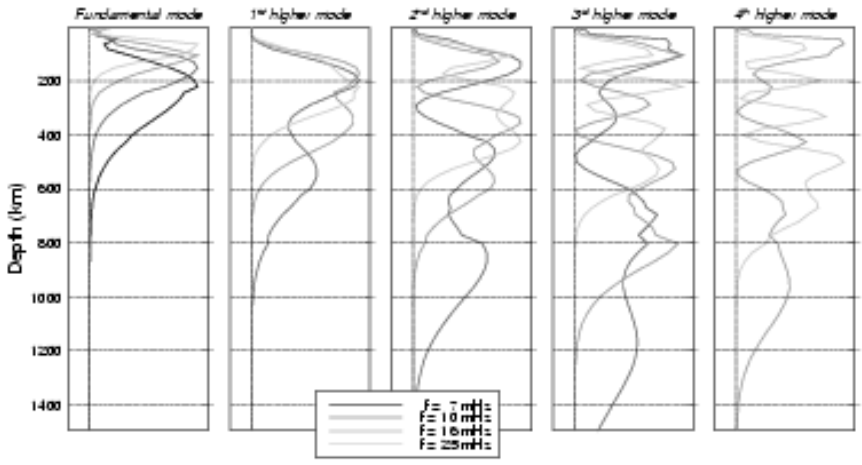

Figure 6: Sensitivity kernels $\left(\frac{\partial c(\omega)}{\partial V_s^0(r)}\right)$ which relate phase velocities of the fundamental and the 1st, 2nd, 3rd, and 4th overtone Rayleigh waves to shear velocity $V_s^0(r)$ for the PREM model.

We analyse the dispersion of Rayleigh waves between 6 mHz and 22 mHz (T = 45–150 s). In addition to the fundamental mode Rayleigh wave, we also analyse overtone Rayleigh waves which constrain seismic structure well below 400 km depth. Analogous to measuring travel times of body waves, we measure the phase velocity of Rayleigh waves by fitting observed ground motion recordings with PREM synthetics. However, this procedure is much more elaborate than the travel time measurement procedure because of the strong Rayleigh wave dispersion and the significant interference of the overtone Rayleigh waves[20,21].

2.3 Normal mode splitting coefficients

Normal mode splitting data provide global constraints on structure in the mantle, and are particularly useful to constrain the amplitude of seismic shear velocity heterogeneity in the mid mantle[22,23]. We incorporate the most extensive set of free-oscillation measurements to date from the study of J. Resovsky and M. Ritzwoller[23].

3 Tomographic inversion

In order to simplify the inversion of the seismic data into a model of seismic shear velocity, we make assumptions regarding wave propagation in the Earth's mantle. In essence, we relate our data to 3-D variations of seismic shear wave speed in the mantle ($V_s(\mathbf{x})$) with respect to the radially symmetric PREM model ($V_s(\mathbf{x}) = V_S^0(r) + \delta V_s(\mathbf{x})$) while we assume that we can describe the propagation of seismic waves using the PREM model. This approximation simplifies the tomographic inversion procedure considerably. First, it renders linear relationships between the data and $\delta V_s(\mathbf{x})$ which can be easily solved on the computer. Second, techniques to compute seismic wave propagation through the PREM model (or other 1-D reference models) are well established. The approximation is useful when we restrict ourselves to studying large-scale (> 1000 km) seismic heterogeneity.

With the linear approximation, the perturbation of surface wave phase velocity, $\delta c(\omega)$, from the PREM-predicted phase velocity is related to $\delta V_s(\mathbf{x})$ by:

$$\delta c(\omega) = \frac{1}{\Delta} \int_L dl \int dr \left(\frac{\partial c(\omega)}{\partial V_s^0(r)} \right) \delta V_s(\mathbf{x}). \tag{1}$$

Here, we have assumed that phase velocity is affected by seismic structure in the mantle beneath the great circle path L (with an arc length of Δ) between source and receiver. Furthermore, we compute sensitivity kernels $\left(\frac{\partial c(\omega)}{\partial V_s^0(r)}\right)$, which relate $c(\omega)$ to $V_s^0(r)$, using the PREM reference model. A linear relationship between normal mode splitting observations and model parameters can be posed in a similar manner[24]. Since Rayleigh wave dispersion and normal mode splitting data are also sensitive to P wave velocities, we assume that S wave velocity and P wave velocity heterogeneity have identical patterns, but that the relative amplitude of S wave velocity anomalies is two times larger. This S-to-P scaling is based on P and S wave travel time data[25].

Travel time perturbations from PREM for seismic shear waves are related to shear velocity perturbations in the following manner:

$$\delta T = \int_{S^0} \frac{ds}{V_s^0(r)} - \int_S \frac{ds}{V_s^0(r) + \delta V_s(\mathbf{x})} \approx - \int_{S^0} \frac{\delta V_s(\mathbf{x})}{V_s^0(r)^2} \, ds. \tag{2}$$

Here, we have assumed that shear waves propagate through the Earth's interior along geometric ray paths S^0 which are computed for the PREM model.

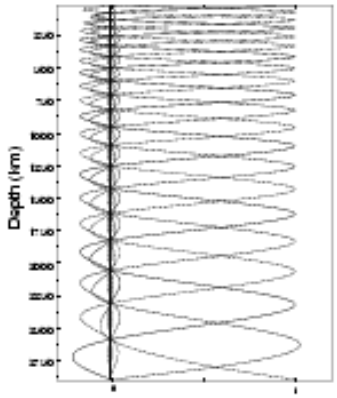

Figure 7: Spline functions used to parameterise the depth dependence of $\delta V_s(\mathbf{x})$.

We parameterize $\delta V_s(\mathbf{x})$, using 21 vertical spline functions (Figure 7) and spherical harmonic functions expanded up to degree 20, which allows for a lateral resolution of shear wave velocity variations with a

half-wavelgnth of about 1000 km:

$$\delta V_s(\mathrm{x}) = \delta V_s(r,\theta,\phi) = \sum_{k}^{21} \sum_{l}^{20} \sum_{m=-l}^{l} m_{klm}\ z_k(r)\ Y_{lm}(\theta,\phi). \tag{3}$$

The spacing of the splines is densest in the uppermost mantle where data coverage is best and where the strongest shear velocity variations are expected. Therefore, vertical resolution of $\delta V_s(\mathrm{x})$ is best in the upper and mid mantle, but it is significantly compromised in the lower mantle, as will be demonstrated in the next section.

The linear relationship between the data and $\delta V_s(\mathrm{x})$ can be denoted in vector form as:

$$\mathrm{d} = G\mathrm{m}, \tag{4}$$

where d is a vector that comprises the Rayleigh phase velocity, free-oscillation spitting, and shear wave travel time measurements, m is a vector of the model elements $\delta V_s(\mathrm{x})$, and G is the matrix that relates data and model according to equations (1) and (2). Using a damped, linear least-squares inversion technique we seek a model m to minimize data misfit and model size simultaneously:

$$(G\mathrm{m} - \mathrm{d})^T (G\mathrm{m} - \mathrm{d}) \text{ and } \epsilon \mathrm{m}^T \mathrm{m}. \tag{5}$$

4 Model S20RTS

Figure 8 shows horizontal cross-sections through S20RTS at eight depths in the mantle. The colour-scale used to present shear velocity heterogeneity varies. Shear velocity variations in the uppermost 200 km of the mantle range from -6% to +6%. They are smaller by up to a factor of 4 in the mid mantle (800–2000 km depth).

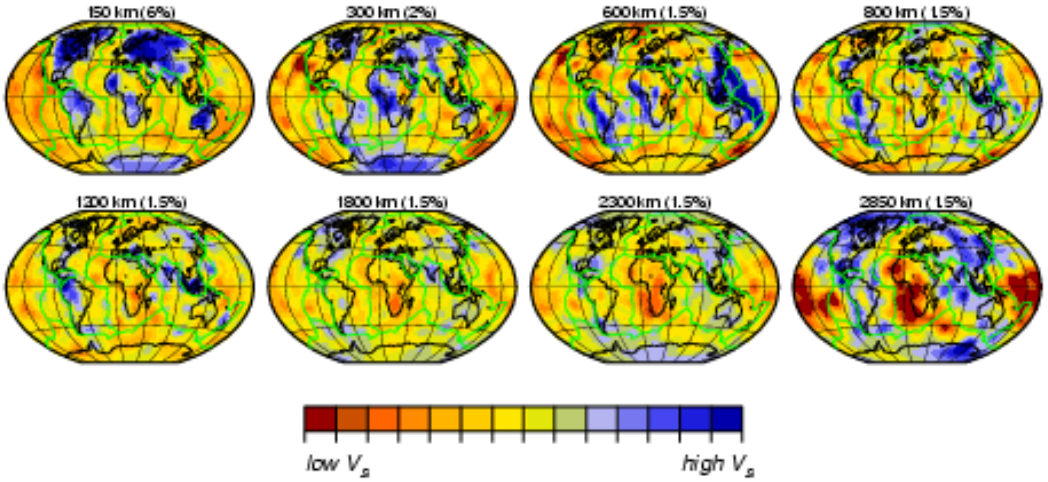

Figure 8: Depth slices through S20RTS. High (relatively to PREM) shear velocity regions are indicated by blue and red colours, respectively, with an intensity that is proportional to the amplitude of the shear velocity perturbations. The range of shear velocity variation (in %) is given above each map. Green lines represent plate boundaries.

Seismic shear velocity heterogeneity in the uppermost mantle ($<$ 250 km) predominantly outlines oceans, continents, and active tectonic regions. Beneath the interior of continental shields (e.g., Canada, Baltic,

western Australia), the shear velocity is up 7% higher than in the PREM model, while shear velocity reductions from PREM are as much as 7% lower than PREM beneath mid-ocean ridges, the Red Sea rift, tectonic western North America, and back-arc regions of subduction zones.

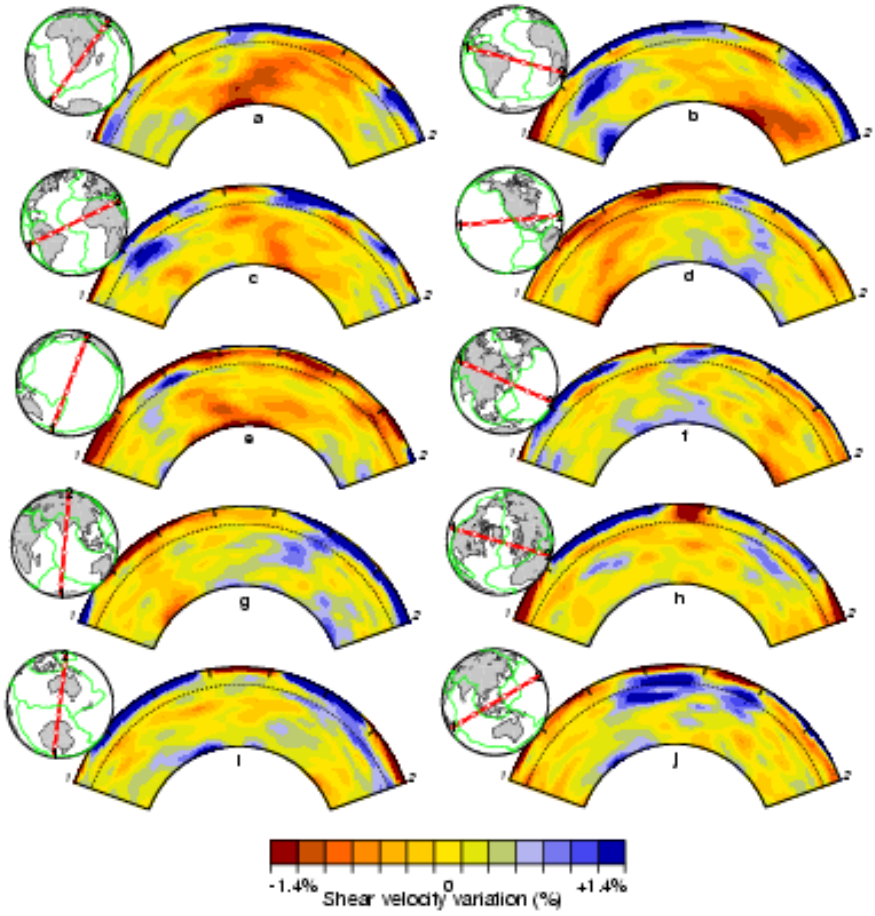

Figure 9: Cross-sections through S20RTS along 140° wide great circle arcs. The representation of shear velocity heterogeneity in the mantle by blue and red colours is the same as in Figure 8. The dashed line represents the 670–km boundary. Superposed are maps showing corresponding great circle arcs along which the cross sections are made. White circles on the arc are plotted at 20° intervals and correspond to the bold tick marks shown in the cross sections.

At 400 km and 600 km depth, the pronounced contrast in shear velocity beneath oceans and continents has disappeared. Elongated high velocity anomalies beneath the western Pacific, South America, and Indonesia are the most dominant structures in this depth range. These structures are most likely due to the presence of relatively cold slabs of former-oceanic lithosphere that have subducted into the upper mantle (> 300 km depth). An equally strong high velocity anomaly beneath Africa is not easily reconciled with plate tectonic processes because subduction in the vicinity of Africa has not occurred since Late Jurassic times (≈ 150 million years ago). We speculate that this high velocity structure is associated with delamination of the

keels of the African cratons during or after the opening of the Atlantic, but a dynamically viable model is yet to be quantified.

The pattern of shear velocity changes abruptly across the spinel-to-perovskite phase transition at a depth of 670 km. While high velocity structures beneath the western Pacific form long continuous structures at 600 km depth, their integrity is lost at 800 km depth. This suggest that the 670–km phase transition impedes the descent of subducting slabs. It appears, however, that the 670–km boundary does not complete obstruct downwellings since high velocity structures beneath Indonesia, Colombia, and the eastern Mediterranean extent to, at least, 1200 km depth.

Except for the lowermost 200 km of the mantle, shear velocity heterogeneity in the lower mantle (670–2890 km depth) is characterised by relatively low-amplitude and small-scale variations. Modestly high shear velocity anomalies are present beneath the Atlantic coast of the Americas, southern and eastern Asia, and Antarctica. The interpretation of these structures as slabs of subducted oceanic lithosphere is consistent with models of subduction during the past 200 million years[28]. Relatively low shear velocity structures emerge beneath southern Africa and the central Pacific Ocean. These structures, associated with large-scale upwelling from the deep mantle, are the most prominent structures in the mantle at depths greater than about 2200 km. Near the core-mantle boundary, the amplitude of shear velocity perturbations from PREM is larger than in the mid mantle.

Figure 9 displays vertical cross-sections through model S20RTS along 140° wide great-circle arcs to further illustrate the variability in radial extent of seismic velocity anomalies in the deep mantle. Broad low velocity anomalies, which likely represent large-scale upwellings that have formed just above the core-mantle boundary, are present beneath Africa (9a,b,c) and the Pacific (9d,e). These anomalies are continuous structures that extend from the core-mantle boundary at least 2000 km into the mantle and are shaped in a complex manner[19]. The vertical extent of high velocity anomalies, presumable signatures of cold downwellings induced by the subduction of oceanic lithosphere, varies strongly geographically. While downwellings beneath North America (9d) and eastern Asia (9f) can be traced from the Earth's surface to the core-mantle boundary[2], high velocity anomalies beneath South America (9b,c), Indonesia, and the Mariana Islands (9j) are characterised by a marked lower boundary at approximately 1200 km depth. The influence of the 670–km boundary is obvious in several cross sections of Figure 9. The 670–km boundary appears to be the lower boundary of an upwelling beneath Iceland (9h). In addition, the amplitude of shear velocity perturbation within high velocity downwellings (9e,f) decreases considerably across the 670–km boundary.

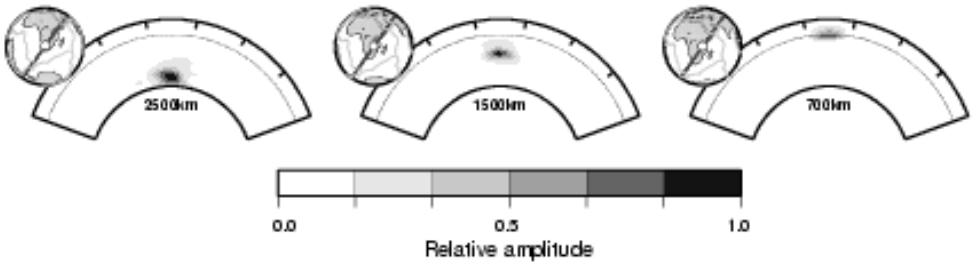

Figure 10: Backus–Gilbert resolution kernels for three locations in the mantle beneath Africa with a relative amplitude ranging from 1/6 (light grey) to 1 (dark grey). Regions where the kernels have a relative amplitude smaller than 1/6 are not shaded.

Backus-Gilbert averaging kernels[27] provide information about how well the model is resolved at various locations in the mantle. A Backus-Gilbert averaging kernel $R(x, x_0)$ is defined by

$$g(x_0) = \int_V dV R(x, x_0) m(x), \tag{6}$$

and describes how the value obtained in the generalized model $g(x_0)$ at x_0 is a spatial average over the

true structure $m(x)$ in the model region V. Ideally, these kernels are spatial delta functions, but given the limited data coverage, finiteness of model parameterisation, and norm damping applied to the inversion these kernels have a finite spatial extent. As an example, we show Backus-Gilbert kernels at three depths in the mantle beneath Africa (Figure 10). While the lateral extent is similar, the radial extent of Backus-Gilbert kernels is largest for the deepest locations in the mantle. The strongly depth dependent vertical resolution, as indicated by the Backus-Gilbert kernels, applies also to other regions. Relatively low model resolution in the deep mantle is due the fact that data coverage is poorest in the deepest regions of the mantle, and, more importantly, due to the fact that the spacing of the spline functions of Figure 7 is largest in the deep mantle. The Backus-Gilbert kernels, however, do not extend across the entire mantle column nor do they reveal a predominantly southwest-northeasterly shape. Therefore, we rule out that the mantle-wide vertical extent of the African anomaly and its tilt, as shown in Figure 9a, is an artifact caused by incomplete data coverage.

5 Concluding remarks

Systematic shear wave velocity variations in the mantle clearly demonstrate the presence of large-scale convection in the mantle. Relatively strong shear wave velocity heterogeneity is present in the uppermost and lowermost 200 km of the mantle. These region represent major boundary layers of mantle convection and are characterised by strong temperature gradients and complex physical processes[28]. Heterogeneity in the mid mantle is considerably weaker.

The spinel-to-perovskite phase transition at a depth of 670 km is a pronounced internal boundary in the mantle that impedes through-going flow: downwellings, visible seismically as relatively high shear velocity anomalies, form long linear structures above the 670–km boundary but this pattern is disrupted below the 670–km boundary. In addition, the 670–km boundary represents a lower boundary of a focussed upper mantle upwelling beneath Iceland.

Given the continuity of high shear wave velocity structures across the 670–km boundary we conclude that the 670–km boundary is not a permanent barrier to mantle flow. For example, relatively strong high shear wave velocity anomalies beneath Indonesia and northern South America extend to about 1200 km depth, while high velocity anomalies, albeit with relatively low amplitude, beneath eastern Asia and North America extend to the core-mantle boundary.

The lower mantle is dominated by broad, low shear velocity upwellings beneath the Pacific Ocean and Africa that extend from the core-mantle boundary at least 2000 km into the mantle. Possibly, these upwellings penetrate into the upper mantle and influence geologic processes at the Earth's surface. The upwelling beneath Africa, for example, may, in part, be responsible for the uplift of the southern African continent and contiguous ocean basins[29,30] and may be linked to continental rifting processes in East Africa[19].

6 Acknowledgments

This research is funded by NSF grant EAR96–96210. Contribution 8713 of the Division of Geological and Planetary Sciences, California Institute of Technology.

7 References

1. Jackson, I. (1998) The Earth's mantle: Composition, Structure, and Evolution. Cambridge University Press, New York.

2. Grand, S.P., Van der Hilst, R.D. & Widiyantoro, S. (1997) Global seismic tomography: A snapshot of convection in the Earth. *GSA Today*, 7, 1–7.

3. Dziewonski, A.M. & Anderson, D.L. (1981) Preliminary reference Earth model. *Phys. Earth Plan. Inter.*, 25, 297–356.

4. Birch, F. (1952) Elasticity and constitution of the Earth's interior. *J. Geophys. Res.*, 57, 227–286.
5. Masters G., Jordan T.J., Silver, P.G. & Gilbert, F. (1982) Aspherical Earth structure from fundamental spheroidal–mode data. *Nature*, 298, 609–613.
6. Nakanishi, I. & Anderson, D.L. (1983) Measurement of mantle wave velocities and inversion for lateral heterogeneity and anisotropy, I, Analysis of great circle phase velocities. *J. Geophys. Res.*, 88, 10,267–10,283.
7. Woodhouse, J.H. & Dziewonski, A.M. (1984) Mapping the upper mantle: Three dimensional modeling of the Earth structure by inversion of seismic waveforms. *J. Geophys. Res.*, 89, 5953–5986.
8. Tanimoto, T. (1990) Long–wavelength S wave velocity structure throughout the mantle. *Geophys. J. Int.*, 100, 327–336.
9. Su, W.-J., Woodward, R.L. & Dziewonski, A.M. (1994) Degree 12 model of shear velocity heterogeneity in the mantle. *J. Geophys. Res.*, 99, 6945–6980.
10. Li, X.-D. & Romanowicz, B. (1996) Global mantle shear velocity model developed using nonlinear asymptotic coupling theory. *J. Geophys. Res.*, 101, 22,245–22,272.
11. Masters, G., Johnson, S., Laske, G. & Bolton., H. (1996) A shear velocity model of the mantle. *Phil Trans. R. Soc. Lon. A*, 354, 1385–1411.
12. Montagner, J.P. (1994) Can seismology tell us anything about convection in the mantle? *Rev. Geophys.*, 32, 115–138.
13. Ritzwoller, M.H. & Lavely, E.M. (1995) Three–dimensional seismic models of the Earth's mantle. *Rev. Geophys.*, 33, 1–66.
14. Van der Lee, S. & Nolet, G. (1997) Upper mantle S velocity structure of North America. *J. Geophys. Res.*, 102, 22,815–22,838.
15. Ritsema, J. & Van Heijst, H. (2000) New seismic model of the upper mantle beneath Africa. *Geology*, 28, 63–66.
16. Zhao, D.P., Du, X.B., Wiens, D.A., Dorman, L., Hildebrand, J. & Webb, S. (1997) Depth extent of the Lau back–arc spreading center and its relation to subduction processes. *Science*, 278, 254–257.
17. Forsyth, D.W., *et al.* (1998) Imaging the deep seismic structure beneath a ridge: The MELT experiment. *Science*, 280, 1215–1218.
18. Van Heijst, H.J., Ritsema, J. & Woodhouse, J.H. (1999) Global P and S velocity structure derived from normal mode splitting, surface wave dispersion, and body wave travel time data. *Eos, Trans. AGU Suppl.*, 80, S221.
19. Ritsema, J., Van Heijst, H.J. & Woodhouse, J.H. (1999) Complex shear wave velocity structure imaged beneath Africa and Iceland. *Science*, 286, 1925–1928.
20. Van Heijst, H.J. & Woodhouse, J.H. (1997) Measuring surface wave overtone phase velocities using a mode branch stripping technique. *Geophys. J. Int.*, 131, 209–230.
21. Van Heijst, H.J. & Woodhouse, J.H. (1999) Global high–resolution phase velocity distribution of overtone and fundamental mode surface waves determined by mode branch stripping. *Geophys. J. Int.*, 137, 601–620.
22. Giardini, D., Li, X.-D. & Woodhouse, J.H. (1987) Three–dimensional structure of the Earth from splitting in free–oscillation data. *Nature*, 325, 405–411.

23. Resovsky, J.S. & Ritzwoller, M.H. (1999) A degree 8 mantle shear velocity model from normal mode observations below 3 mHz. *J. Geophys. Res.*, 104, 993–1014.

24. Woodhouse, J.H. & Girnius, T.P. (1982) Surface waves and free oscillations in a regionalised Earth model. *Geophys. J. R. astr. Soc.*, 68, 653–673.

25. Robertson, G.S. & Woodhouse, J.H. (1995) Evidence for proportionality of P and S heterogeneity in the lower mantle. *Geophys. J. Int.*, 123, 85–116.

26. Lithgow–Bertelloni, C. & Richards, M.A. (1998) The dynamics of Cenozoic and Mesozoic plate motions. *Rev Geophys.*, 36, 27–78.

27. Backus, G.E. & Gilbert, J.F. (1962) The resolving power of gross Earth data. *Geophys. J. R. astr. Soc.*, 16, 169–205.

28. Lay, T., Williams, Q. & Garnero, E.J. (1998) The core-mantle boundary layer and deep Earth dynamics. *Nature*, 392, 461–468.

29. Hager, B.H., Clayton, R.W., Richards, M.A., Comer, R.P. & Dziewonski, A.M. (1985) Lower mantle heterogeneity, dynamic topography and the geoid. *Nature*, 313, 541–545.

30. Gurnis, M., Mitrovica, J.X., Ritsema, J. & van Heijst, H.J. (2000) Constraining mantle density structure using geological evidence of surface uplift rates: The case of the African superplume. *Geochem. Geophys. Geosys.*, in press.